Optik - International Journal for Light and Electron Optics 272 (2023) 170323

Contents lists available at ScienceDirect

Optik

journal homepage: www.elsevier.com/locate/ijleo

Steering of one-way large-area waveguide modes in topological heterostructures with gyromagnetic photonic crystals

Liu He [a], Qun Ren [b,c], Jian Wei You [c], Wei E.I. Sha [d], Zhihao Lan [e], Yating Zhang [a,*], Jianquan Yao [a,f,*]

[a] Key Laboratory of Opto-Electronics Information Technology (Tianjin University), Ministry of Education, School of Precision Instruments and Opto-Electronics Engineering, Tianjin University, Tianjin 300072, China
[b] School of Electrical and Information Engineering, Tianjin University, Tianjin 300072, China
[c] State Key Laboratory of Millimeter Waves, School of Information Science and Engineering, Southeast University, Nanjing 210096, China
[d] Key Laboratory of Micro-Nano Electronic Devices and Smart Systems of Zhejiang Province, College of Information Science and Electronic Engineering, Zhejiang University, Hangzhou 310027, China
[e] Department of Electronic and Electrical Engineering, University College London, Torrington Place, London WC1E 7JE, United Kingdom
[f] Department of Electrical and Electronic Engineering, South University of Science and Technology of China, Shenzhen 518055, China

ARTICLE INFO

Keywords:
Magnetic-optical photonic crystals
Topological heterostructures
One-way large-area waveguide modes
Multifunctional steering

ABSTRACT

We study the steering of one-way and large-area topological waveguide modes in heterostructures consisting of a domain of ordinary photonic crystals sandwiched between two domains of magnetic-optical photonic crystals. Taking advantage of the band and mode properties of the topological heterostructures, we first demonstrate the design of four basic steering units which can realize the functionalities of forward-guiding, T-splitting, upward turning and downward turning. We demonstrate in detailed characteristic with the high-efficiency and broad-bandwidth of these basic steering units designed. Moreover, by combining these basic steering units, we implement a series of multifunctional waveguide devices, such as one-way large-area waveguide splitters with multiple channels and different angles, a highly bended large-area waveguide with five 90° corners along the propagation path, and waveguide structures supporting waveguide-cavity interaction, delay, splitting as well as storage functionalities. Importantly, all these different functionaries could be realized in a single system platform by simply reconfiguring the underlying magnetic field distributions. Our work opens up a new venue towards designing multi-functional waveguide devices by exploiting the width degree of freedom of the large-area waveguide modes.

1. Introduction

Topological insulators have emerged as one of the most important research topics in condensed matter physics during the past decades [1,2]. These novel insulating materials host gapped bulk states but gapless edge states, which reside within the band gap and exhibit robust unidirectional transport immune to imperfections or defects caused by disorder and sharp bends, providing a unique opportunity for robust wave manipulations due to topological protection. Haldane and Raghu [3] were the first to propose analogs of

* Correspondence to: Tianjin University, School of Precision Instruments and Opto–Electronics Engineering, No. 92, Weijin Road, Nankai district, Tianjin 300072, China.
E-mail addresses: yating@tju.edu.cn (Y. Zhang), jqyao@tju.edu.cn (J. Yao).

https://doi.org/10.1016/j.ijleo.2022.170323
Received 16 September 2022; Received in revised form 9 November 2022; Accepted 29 November 2022
Available online 1 December 2022

quantum Hall edge states for electromagnetic waves in photonic crystals with broken time-reversal symmetry, which were experimentally demonstrated later on by Wang et al. [4,5], who have observed such chiral backscattering-immune topological electromagnetic states in magneto-optical photonic crystals (MOPCs). MOPCs are usually composed of gyromagnetic materials, whose magnetic permeability tensor shows imaginary off-diagonal terms under external bias magnetic fields [6]. As a result, the time-reversal (TR) symmetry of such systems made of MOPCs is broken by the magneto-optical (MO) effect under external magnetic fields, enabling non-reciprocal one-way transport of electromagnetic waves. Moreover, the number of one-way edge states within the topological band gap is determined by the Chern number and large Chern numbers in MOPCs have been demonstrated [7].

The one-way backscattering-immune topological electromagnetic modes realized in MOPCs have opened up a broad range of applications [8,9], such as tunable one-way cross-waveguide splitter [10], unidirectional channel-drop filter [11], self-guiding unidirectional electromagnetic edge states [12,13], topological slow-light [14–18], unpaired photonic Dirac point [19], topological lasing in cavities of arbitrary geometries [20], nonlinear frequency mixing [21,22], and topological states as well as phase transitions in amorphous or disordered MOPCs [23–27]. While the one-way topological electromagnetic modes in most works were studied at the interface between two PC structures with different topological properties, very recently, large-area topological waveguide states based on three-layer heterostructures have been proposed and studied both in photonics [28–30] and acoustics [31–33], opening a new venue for manipulating topological waveguide modes by adding the width of the waveguide modes as a new degree of freedom, which could be adjusted flexibly.

Here we demonstrate the steering of one-way large-area topological waveguide modes in a domain of trivial PCs with finite width sandwiched between two domains of MOPCs. Especially, we first show that four basic functionalities, i.e., forward-guiding, T-splitting, upward turning and downward turning, could be realized in such topological heterostructure by properly configuring the external bias magnetic fields. Furthermore, based on these four basic functionalities, more complicated and advanced functionalities, such as one-way large-area waveguide splitters with multi-channel and different-angle, a highly bended large-area waveguide with five 90° corners along the propagation path, high-energy-capacity topological channel intersection and topological cavities with the ability to interact with waveguide and store energy, could be realized. The demonstration of effective on-demand steering of one-way large-area topological waveguide states may find promising applications in nonreciprocity-based multifunctional waveguide devices with flexible configurability [34–37] by coding (see in supplementary material in detail) the underlying bias magnetic fields.

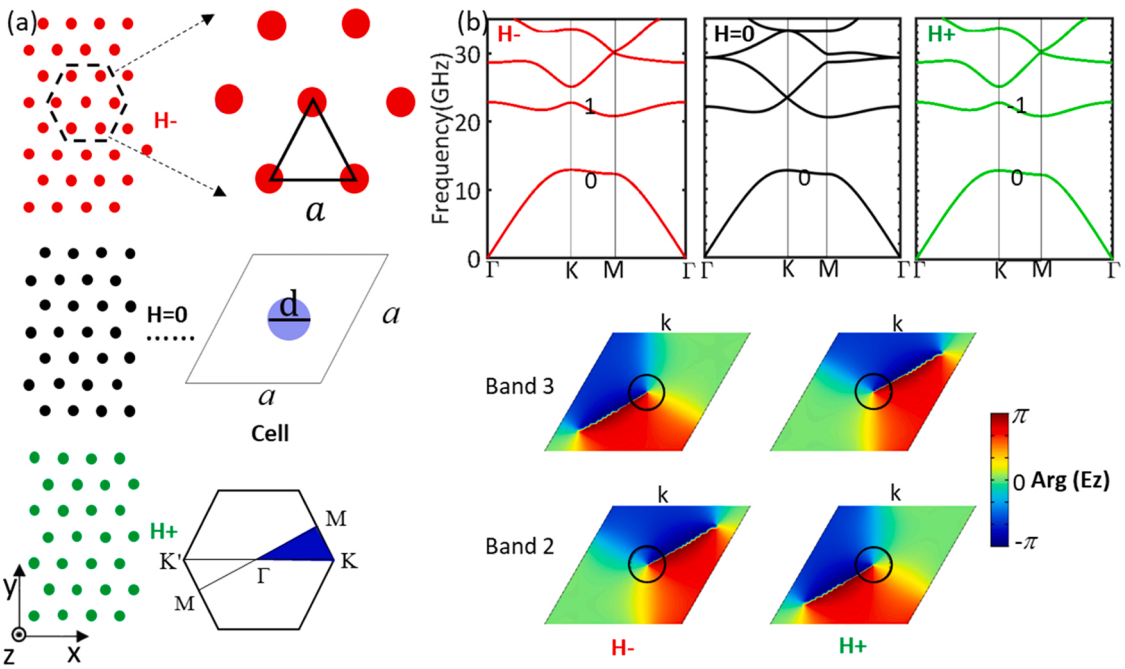

Fig. 1. (Color online) (a) Schematic of the three domains of MOPCs used to construct the topological heterostructure, where the lattice constant is a= 8 mm and the cylinder diameter is $d = 0.25a$. The red, black and green rods denote the domains with a magnetic field applied along the –z direction, without magnetic field and with a magnetic field applied along the +z direction, respectively. (b) Bulk band structures of the three domains for H-, H0, and H+ , respectively. The Chern numbers corresponding to the first two bands are labeled. The bottom panels show the phase distributions of the electric fields (Ez) of the second and third bands at the K point for H- and H+ , respectively.

2. Model system

2.1. Structure and parameters of the topological heterostructure

The model system we considered in this work is made of gyromagnetic PCs with cylindrical yttrium iron garnet (YIG) rods arranged in triangular lattices [30], where the lattice constant a is 8 mm; the radius and the relative permittivity of the YIG rods is 0.125 a and 13.8, respectively. Without the external bias magnetic fields, the magnetic permeability of the YIG rods is μ_0, which could be regarded as all-dielectric materials. Under an external bias magnetic field along the +z direction (out-of-plane), the relative magnetic permeability of the YIG rods shows a second-rank tensor form, which could be written as following [6].

$$\overline{\mu} = \begin{bmatrix} \mu_r & j\kappa & 0 \\ -j\kappa & \mu_r & 0 \\ 0 & 0 & 1 \end{bmatrix} \left(+z \text{ bias} \right)$$

Where $\mu_r = 1 + \frac{\omega_0^{'}\omega_m}{\omega_0^{'2}-\omega^2}$, $\kappa = \frac{\omega\omega_m}{\omega_0^{'2}-\omega^2}$, $\omega_0^{'} = \omega_0 + i\alpha\omega$with α the damping factor. The characteristic frequency$\omega_0 = \gamma H_0$, and $\omega_m = 4\pi\gamma M_s$ with the saturation magnetization $4\pi M_s = 1850$G (gauss) and gyromagnetic ratio $\gamma = 2.8$ MHz/Oe. In this work, we consider $\alpha = 0.0002, H_0 = 835Oe$, $H = 4285.7Oe$, $\omega = 12$ GHz, $\mu_r = 0.9126$, $\kappa = 0.4487$.

2.2. Topological properties of the MOPCs

The topological heterostructure consists of a domain of trivial PCs sandwiched between two domains of MOPCs (see Fig. 1(a)), where the red YIG rods denote the domain with a direct current (dc) magnetic field applied along the -z direction, the black YIG rods denote the domain without magnetic field applied, and the green YIG rods denote the domain with a dc magnetic field applied along the +z direction, respectively. Here Let us consider harmonic TM modes of the EM waves, namely, those of finite out-of-plane Ez and in-plane Hx and Hy components with others being zero [9]. The band structure of the three domains with different magnetic fields (H-, H0, H+) are shown in Fig. 1(b). From the band diagram without magnetic field (i.e., H0), one can see that the second and third bands are degenerated and forming a ''Dirac point'' at the K point of the first Brillouin zone. When an external magnetic field is applied along the -z direction (H-) or +z direction (H+), the Dirac point between the second and third bands is gapped out, leading to a photonic band gap (PBG). To demonstrate that the band gap obtained by gapping out the Dirac point is topological, we calculate the Chern numbers of

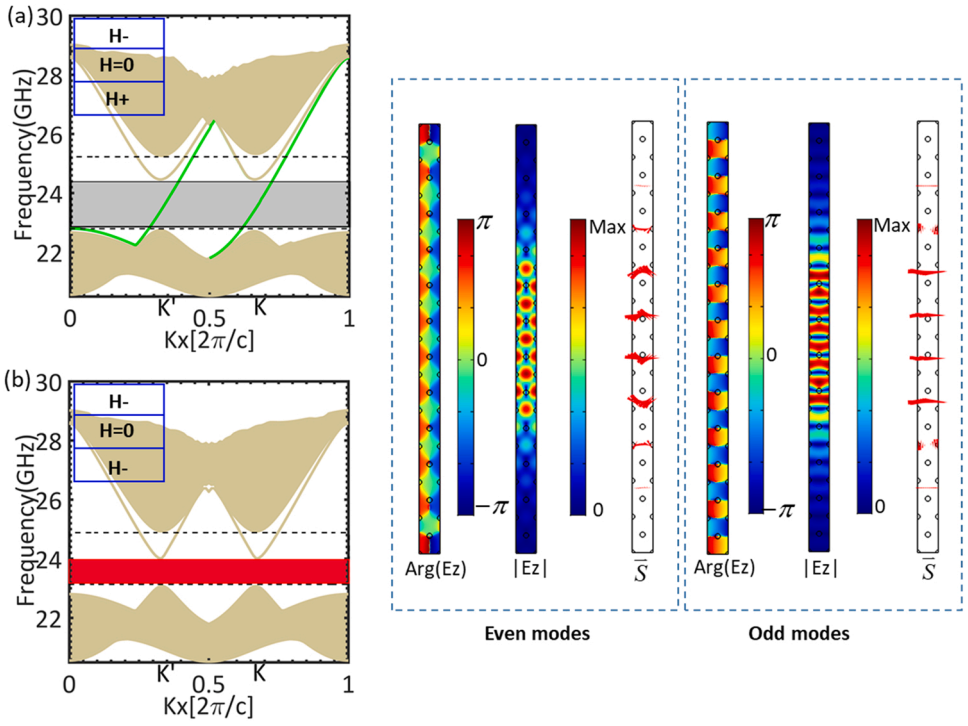

Fig. 2. (Color online) (a) Projected band structure of the heterostructure configured by H-/H0/H+ along kx, which shows gapless waveguide mode dispersion. (b) Projected band structure of the heterostructure configured by H-/H0/H- along kx, which shows gapped waveguide mode dispersion. (c) The phase distributions and amplitude of Ez fields, and Poynting vectors distributions of the edge states at K′ and K points (i.e., (1/3, 23.526) and (2/3, 23.526)) in (a), respectively.

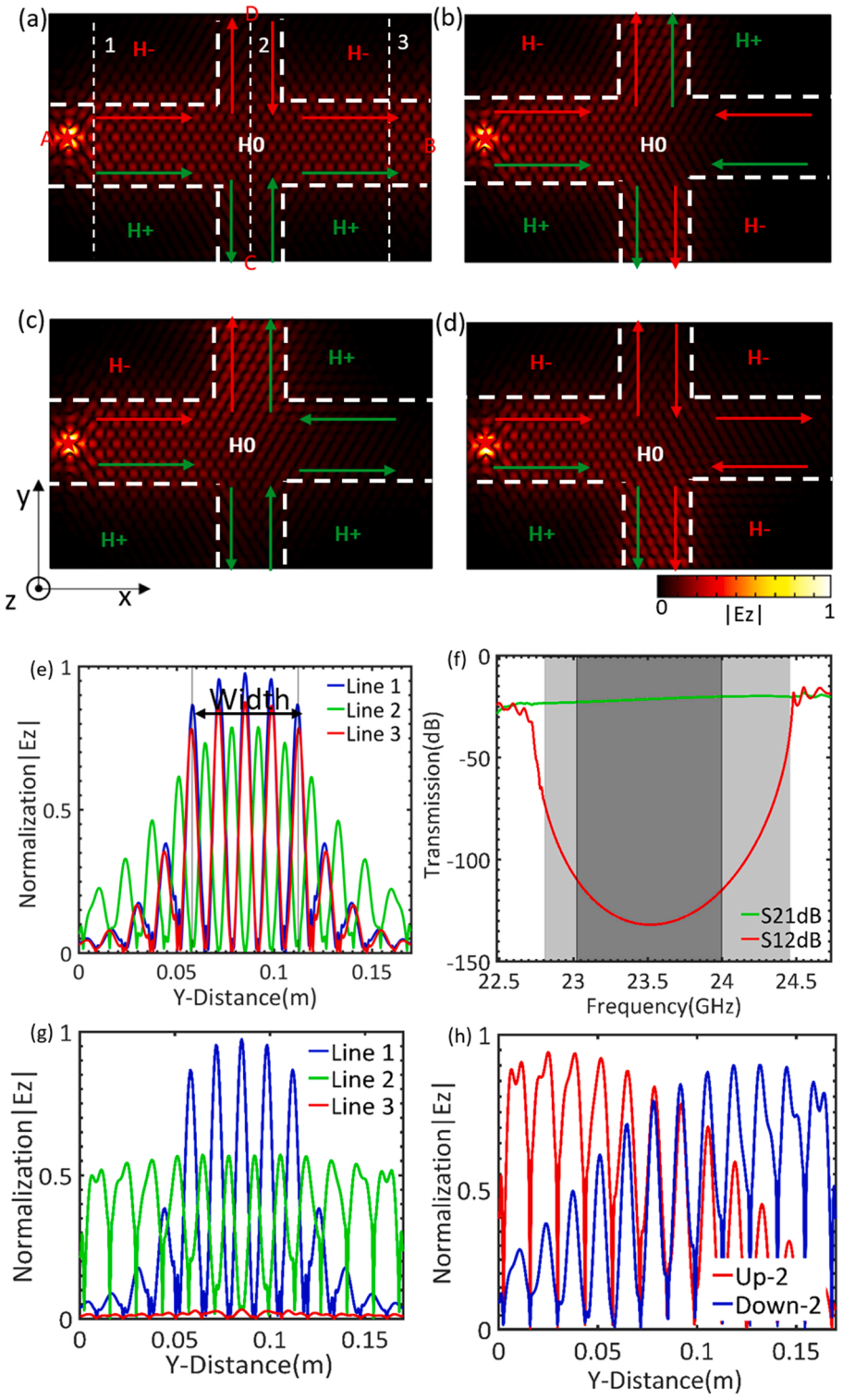

Fig. 3. (Color online) (a)–(d) Field distributions of the Ez field for the four waveguide structures, realizing forward-guiding, T-splitting, upward turning and downward turning at 23.635 GHz. Here, A, B, C and D denote the waveguide channels and the bold dashed lines denote the interfaces between different domains. The arrows denote the propagation directions of the edge modes supported at the interface between H-/H0 or H+ /H0. The red star denotes the location of the excitation source. (e) Normalized |Ez| along the thin dashed white lines in (a). (f) Simulated transmission spectra upon the forward and backward transmissions. (g) Normalized |Ez| corresponding to (b). (h) Normalized |Ez| corresponding to (c) and (d).

the first two bands [38], which are labeled in Fig. 1(b). As the topological property of band gap is determined by the sum of the Chern number of all bands below that band gap, it can be inferred that the band gaps of the red and green domains have a nontrivial gap Chern number of 1 and − 1, respectively. Additionally, the phase distributions of the electric fields (Ez) of the second and third bands at K point are also given, from which one can see that the phases at K point of the second and third bands wind along opposite directions for both H- and H+ , as shown at the bottom of Fig. 1(b).

2.3. Projected band structures and large-area topological modes of the heterostructure

The projected band structure of the three-layer heterostructure configured by H-/H0/H+ are calculated and presented in Fig. 2(a), where the waveguide modes are colored by green whereas the shaded grey area denotes the operation frequency range (from 22.81 GHz to 24.46 GHz) and the area between two black dashed lines is the range of bulk gap for H- and H+ . To demonstrate that these waveguide modes are indeed large-area topological modes confined within the middle domain, we choose an eigenfrequency around the K′ and K points in the waveguide modes. From the corresponding electric field distributions presented in Fig. 2(c), it can be observed that the electric fields (Ez) are highly localized in the middle black domain, i.e., in the domain without magnetic field applied for both the even and odd modes. From the Poynting vectors distributions depicted in red arrows, it can be observed that electric fields energy are not only highly concentrated in the domain H0 but also shows unidirectionality. To further show the possibility to switch off these large area waveguide modes, we calculate and present the projected band structure of the heterostructure configured by H-/H0/H- in the Fig. 2(b), from which one can observe that there is a band gap (shaded red area) within the operation bandwidth (the shaded light gray area), i.e., these large-area waveguide modes are prohibited within the band gap from 23.08 GHz to 23.98 GHz.

3. Results and discussions

3.1. Four fundamental functionalities

Based on the mode properties of the heterostructure discussed above, we could construct four basic waveguide structures to realize four fundamental functionalities, i.e., forward-guiding, T-splitting, upward turning and downward turning (see Fig. 3(a)-(d)), which could be used to realize more complicated and advanced functionalities.

In the four waveguide structures shown in Fig. 3(a)-(d), the configurations of the magnetic fields are shown and marked by H-, H+ and H0 and it can be seen that the one-way large-area waveguide states are mainly confined to the H0 domain (7 layers along the y direction), which is due to the strong interaction between the two co-propagating topological one-way edge states supported at the interface between H-/H0 and H+ /H0 (the propagation directions of these edge states are marked by red and green arrows). Especially, while the one-way large-area waveguide states are mainly propagating within the channel A and B when the frequency is around 23.635 GHz (see Fig. 3(a)), these states are completely blocked in channel B (see Fig. 3(b)), forming a splitting functionality. Similarly, by configuring the applied magnetic fields, one could also redirect the waveguide mode from channel A to either C (downward turning, Fig. 3(c)) or D (upward turning, Fig. 3(d)).

3.2. Detailed characterizations of the four basic waveguide structures

To quantify the performance of the four basic waveguide structures shown in Fig. 3(a-d), we study the Ez fields along y-direction at three different propagation distances $(2a, 18a, 34a)$ () as marked by line 1, line 2, and line 3 in Fig. 3(a). For the case of forward-guiding, from the results shown in Fig. 3(e), one can see that the field distributions are evenly distributed within the H0 domain with a width of $(7 \times \sqrt{3}/2a)$, and away from domain H0, the fields show a fast decay to both domain H- and H+ . The result of Ez fields along line 2 shows that the field has a small spread to channels C and D due to a fact that the waveguide states in channel C and D are completely prohibited because the corresponding frequency is within the completely photonic band gap (marked by red area in Fig. 2 (b)). We would like to note that the waveguide states studied here are different from the slow light states studied previously [16,17], which is due to the strong interaction between the two counter-propagating topological unidirectional edge states supported at the interface between two semi-infinite MOPCs and the resulting slow light states show flat and self-trapping photonic bands [15,39] and thus do not possess the properties of transport or splitting. Moreover, from the results of Ez fields along line 1 and line 3, we can see that the offset between them are very small within the H0 domain even if they are located $36a$ apart along the propagation distance, indicating that the transport of these one-way large-area waveguide states is very efficient.

We further use the S-parameter to measure transmission specific feature for the forward and backward transmissions with the simulated transmission spectra (transmission (dB) against frequency (GHz)) being shown in Fig. 3(f), where the shaded light gray region denotes the operation bandwidth, whereas the shaded dark gray region denotes the band gap. The difference between transmission spectra in the forward and backward directions is called isolation in the literature, which could be used as a useful guidance for designing waveguide devices [40]. We find that the larger of the difference between the transmission spectra in the forward and backward directions is, more strong nonreciprocity of the waveguide transmission will be, and the optimal operation frequency range is approximately from 23.08 GHz to 23.98 GHz, which agrees with the above analysis.

From the results of the T-splitting shown in Fig. 3(g), one can see that the electric field Ez is evenly distributed within the domain H0 in channel A along line 1 whereas channels C and D receive 50% of the total energy (see the result indicated by line 2) and there is no energy transmitted to channel B (see the result indicated by line 3). The fact that the wave can propagate in channel A but not in

channel B agrees with the mode properties discussed above (for the distributions of Poynting vectors, see Supplemental Material). Similarly, from the results of upward turning and downward turning shown in Fig. 3(h), one can see that the energy is either directed to channel D or C. These detailed characterizations demonstrate that the four basic waveguide structures can achieve the target functionalities using one-way large-area topological waveguide modes with high-efficiency and broad-bandwidth.

3.3. Multifunctional steering

To demonstrate the great potential of realizing more complicated and advanced functionalities by steering the large-area topological waveguide modes based on the four basic functionalities discussed above, here, we implement several multi-functional waveguide devices (see Fig. 4) by combining the different functionalities discussed above. In specific, in Fig. 4(a), a four-port T-splitting device is constructed, where each T-splitting unit can equally divide the energy into two and in Fig. 4(b), a four-port V-splitting is designed, from which one can see that the one-way large-area waveguide states are immune to any bends. To further demonstrate that the wave propagation path could be configured arbitrarily, we design a large-area waveguide structure with five 90° corners along the propagation path, as shown in Fig. 4(c). Moreover, topological waveguide structures based on the interaction between waveguide and cavity could also be realized, e.g., as demonstrated in Fig. 4(d). Fig. 4(e) shows a one-way large-area delay waveguide while Fig. 4(f) shows the design of a waveguide device with both splitting and storage functionalities. We would like to note that in the simulations of Fig. 4(f), a slab of perfect electrical conductor (PEC) with width $10\sqrt{3}a$ and thickness $0.05a$ marked by the black lines is used to prevent the energy from leaking out along the interface between different domains (for the distributions of Poynting vectors in these devices, see Supplemental Material). The different functionalities achieved in the waveguide devices discussed above could be realized in a single system platform by reconfiguring the underlying magnetic field distributions. We believe these multifunctional waveguide devices based on the steering of large-area topological waveguide modes could serve as a novel

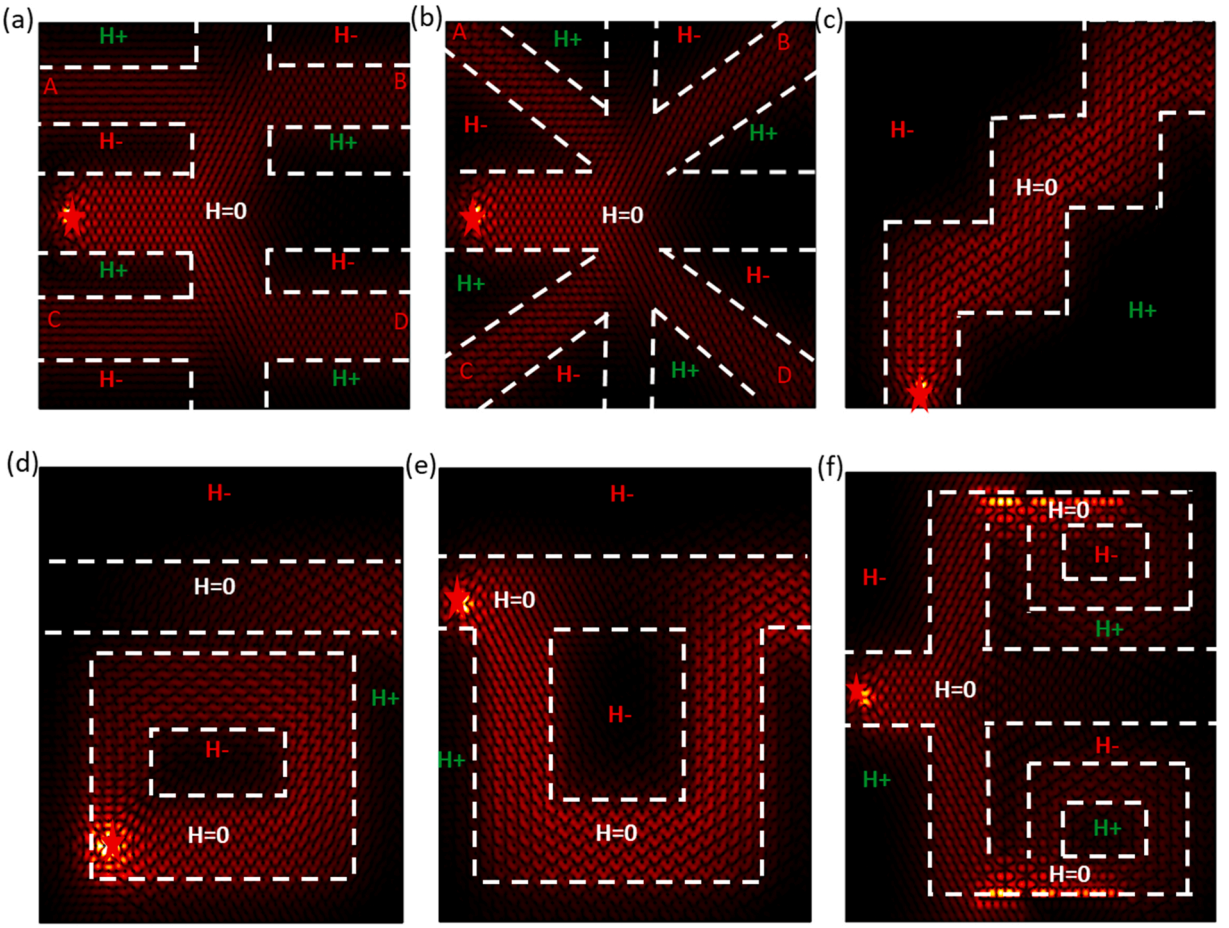

Fig. 4. (Color online) (a) Field distributions of the Ez fields of a four-port T-splitting structure. (b) Filed distributions of the Ez fields of a four-port V-splitting structure. (c) Field distributions of the Ez fields of along a path with five 90° corners. (d) Field distributions of the Ez fields of a structure supporting waveguide-cavity interaction. (e) Field distributions of the Ez fields of a structure with delay. (f) Field distributions of the Ez fields of a structure with splitting and storage.

platform for practical applications, e.g., field enhancement and high-capacity energy transport [29]. Additionally, in experimental setup, we need prepare two aluminum plates containing holes drilled in a way to meet the lattice of the MOPCs, which is used to clad the MOPCs (top and bottom). Lots of permanent magnet NdFeB pillars with the corresponding polarities are embedded into the holes in magnetized domains (H+/H- domain), in order to magnetize the YIG rods. There is test system with an emitter and detector. For experimental processing and steps, we can see supplementary materials in detail.

4. Conclusion

In conclusion, we have investigated the steering of one-way large-area topological waveguide modes in topological heterostructures consisting of a domain of ordinary PCs sandwiched between two domains of MOPCs. We first characterized these large-area topological waveguide states through band and mode analysis. We then constructed four basic steering units that can achieve four functionalities of forward-guiding, T-splitting, upward turning and downward turning and characterized the performance of these four basis units in detail, demonstrating the high-efficiency and broad-bandwidth of the designed structures. Moreover, to show the great potential of steering these large-area waveguide states in more complicated situations for more advanced functionalities and applications, we have implemented a series of multifunctional waveguide devices by combining the four basic steering units, such as, one-way large-area waveguide splitters with multi-channel and different-angle, a highly bended large-area waveguide with five 90° corners along the propagation path, a topological waveguide device supporting waveguide-cavity interaction, a topological waveguide structure with delay functionality, and a structure support splitting and storage functionality. More importantly, the different functionaries described in our work could be realized in a single system platform by simply reconfiguring the underlying magnetic field distributions. The topological waveguide modes with tunable width may provide a promising and platform for practical use of topological waveguide devices, such as field enhancement, a topological concentrator, and high-capacity energy transport.

CRediT authorship contribution statement

Liu He: Investigation, Writing – original draft, Validation, Formal analysis. **Qun Ren:** Conceptualization, Writing – review & editing. **Jian Wei You:** Conceptualization, Writing – review & editing. **Wei E. I. Sha:** Investigation, Writing – review & editing. **Zhihao Lan**: Investigation, Writing – review & editing. **Yating Zhang:** Investigation, Writing – review & editing, Project administration. **Jianquan Yao**: Conceptualization, Supervision, Funding acquisition. All authors have read and agreed to the published version of the manuscript.

Declaration of Competing Interest

The authors declare that they have no known competing financial interests or personal relationships that could have appeared to influence the work reported in this paper.

Data Availability

Data will be made available on request.

Acknowledgements

This work was supported by the National Key Research and Development Program of China (No. 2021YFB2800703 and 2017YFA0700202), the National Natural Science Foundation of China (No. 61735010) and Basic Research Program of Shenzhen (JCYJ20170412154447469).

References

[1] M.Z. Hasan, C.L. Kane, Colloquium: topological insulators, Rev. Mod. Phys. 82 (2010) 3045.
[2] X.L. Qi, S.C. Zhang, Topological insulators and superconductors, Rev. Mod. Phys. 83 (2011) 1057.
[3] F.D. Haldane, S. Raghu, Possible realization of directional optical waveguides in photonic crystals with broken time-reversal symmetry, Phys. Rev. Lett. 100 (2008), 013904.
[4] Z. Wang, Y.D. Chong, J.D. Joannopoulos, M. Soljacic, Reflection-free one-way edge modes in a gyromagnetic photonic crystal, Phys. Rev. Lett. 100 (2008), 013905.
[5] Z. Wang, Y.D. Chong, J.D. Joannopoulos, M. Soljacic, Observation of unidirectional backscattering-immune topological electromagnetic states, Nature 461 (2009) 772.
[6] D.M. Pozar. Microwave Engineering, fourth ed., Wiley, NewYork, 1998.
[7] S.A. Skirlo, L. Lu, Y. Igarashi, Q.H. Yan, J. Joannopoulos, M. Soljačić, Experimental observation of large chern numbers in photonic crystals, Phys. Rev. Lett. 115 (2015), 253901.
[8] X. Wang, W. Zhao, H. Zhang, S. Elshahat, C. Lu, Magnetic-optic effect-based topological state: realization and application, Front. Mater. 8 (2022), 816877.
[9] Z. Lan, M.L.N. Chen, F. Gao, S. Zhang, W.E.I. Sha, A brief review of topological photonics in one, two, and three dimensions, Rev. Phys. 9 (2022), 100076.
[10] C. He, X.L. Chen, M.H. Lu, X.F. Li, et al., Tunable one-way cross-waveguide splitter based on gyromagnetic photonic crystal, Appl. Phys. Lett. 96 (2010), 111111.
[11] J.X. Fu, J. Lian, R.J. Liu, L. Gan, Z.Y. Li, Unidirectional channel-drop filter by one-way gyromagnetic photonic crystal waveguides, Appl. Phys. Lett. 98 (2011), 211104.
[12] X.Y. Ao, Z.F. Lin, C.T. Chan, One-way edge mode in a magneto-optical honeycomb photonic crystal, Phys. Rev. B. 80 (2009), 033105.

[13] Y. Poo, R.X. Wu, Z. Lin, Y. Yang, C.T. Chan, Experimental realization of self-guiding unidirectional electromagnetic edge states, Phys. Rev. Lett. 106 (2011), 093903.
[14] Y. Yang, Y. Poo, R.X. Wu, Y. Gu, P. Chen, Experimental demonstration of one-way slow wave in waveguide involving gyromagnetic photonic crystals, Appl. Phys. Lett. 102 (2013), 231113.
[15] Y.T. Fang, H.Q. He, J.X. Hu, L.K. Chen, Z. Wen, Flat and self-trapping photonic bands through coupling of two unidirectional edge modes, Phys. Rev. A. 91 (2015), 033827.
[16] J.F. Chen, W.Y. Liang, Z.Y. Li, Strong coupling of topological edge states enabling group-dispersionless slow light in magneto-optical photonic crystals, Phys. Rev. B. 99 (2018), 014103.
[17] J.F. Chen, W.Y. Liang, Z.Y. Li, Switchable slow light rainbow trapping and releasing in strongly coupling topological photonic systems, Photonics Res 7 (2019) 1075.
[18] S.N. Zhuang, J.F. Chen, W.Y. Liang, Z.Y. Li, Zero GVD slow-light originating from a strong coupling of one-way modes in double-channel magneto-optical photonic crystal waveguides, Opt. Express 29 (2021) 2478.
[19] G.G. Liu, P. Zhou, Y. Yang, H. Xue, X. Ren, X. Lin, H.-X. Sun, L. Bi, Y. Chong, B. Zhang, Observation of an unpaired photonic Dirac point, Nat. Commun. 11 (2020) 1873.
[20] B. Bahari, A. Ndao, F. Vallini, A. El Amili, Y. Fainman, B. Kante, Nonreciprocal lasing in topological cavities of arbitrary geometries, Science 358 (2017) 636–640.
[21] J.W. You, Z. Lan, N.C. Panoiu, Four-wave mixing of topological edge plasmons in graphene metasurfaces, Sci. Adv. 6 (2020) eaaz3910.
[22] Z. Lan, J.W. You, N.C. Panoiu, Nonlinear one-way edge-mode interactions for frequency mixing in topological photonic crystals, Phys. Rev. B 101 (2020), 155422.
[23] S. Mansha, Y.D. Chong, Robust edge states in amorphous gyromagnetic photonic lattices, Phys. Rev. B 96 (2017), 121405(R).
[24] B. Yang, H. Zhang, T. Wu, R. Dong, X. Yan, X. Zhang, Topological states in amorphous magnetic photonic lattices, Phys. Rev. B 99 (2019), 045307.
[25] B. Yang, H. Zhang, Q. Shi, T. Wu, Y. Ma, Z. Lv, X. Xiao, R. Dong, X. Yan, X. Zhang, Details of the topological state transition induced by gradually increased disorder in photonic Chern insulators, Opt. Express 28 (2020) 31487–31498.
[26] G.G. Liu, Y. Y, X. Ren, H. Xue, X. Lin, Y.H. Hu, H.X. Sun, B. Peng, P. Zhou, Y. Chong, B. Zhang, Topological Anderson Insulator in Disordered Photonic Crystals, Phys. Rev. Lett. 125 (2020), 133603.
[27] P. Zhou, G.G. Liu, X. Ren, Y. Yang, Y. Chong, B. Zhang, Photonic amorphous topological insulator, Light Sci. Appl. 9 (2020) 133.
[28] L. He, H.Y. Ji, Y.J. Wang, X.D. Zhang, Topologically protected beam splitters and logic gates based on two-dimensional silicon photonic crystal slabs, Opt. Express 28 (2020) 34015–34023.
[29] Q. Chen, L. Zhang, F. Chen, Q. Yan, R. Xi, H. Chen, Y. Yang, Photonic topological valley-locked waveguides, ACS Photonics 8 (2021) 1400.
[30] M.D. Wang, R.Y. Zhang, L. Zhang, D. Wang, Q. Guo, Z.Q. Zhang, C.T. Chan, Topological one-way large-area waveguide states in magnetic photonic crystals, Phys. Rev. Lett. 126 (2021), 067401.
[31] M. Wang, W. Zhou, L. Bi, C. Qiu, M. Ke, Z. Liu, Valley-locked waveguide transport in acoustic heterostructures, Nat. Commun. 11 (2020) 3000.
[32] J.Q. Wang, Z.D. Zhang, S.Y. Yu, H. Ge, K.F. Liu, T. Wu, X.C. Sun, L. Liu, H.Y. Chen, C. He, M.H. Lu, Y.F. Chen, Extended topological valley-locked surface acoustic waves, Nat. Commun. 13 (2022) 1324.
[33] Z. Chen, X. Wang, C.W. Lim, F. Shi, Robust large-area elastic transverse wave transport in active acoustic metamaterials, J. Appl. Phys. 131 (2022), 185112.
[34] X. Cheng, C. Jouvaud, X. Ni, S.H. Mousavi, A.Z. Genack, A.B. Khanikaev, Robust reconfigurable electromagnetic pathways within a photonic topological insulator, Nat. Mater. 15 (2016) 542–548.
[35] J.P. Xia, D. Jia, H.X. Sun, S.Q. Yuan, Y. Ge, Q.R. Si, X.J. Liu, Programmable coding acoustic topological insulator, Adv. Mater. 30 (2018), e1805002.
[36] A. Darabia, M. Colletb, M.J. Leamy, Experimental realization of a reconfigurable electroacoustic topological insulator, PNAS 117 (2020) 16138–16142.
[37] J.W. You, Q. Ma, Z. Lan, Q. Xiao, N.C. Panoiu, T.J. Cui, Reprogrammable plasmonic topological insulators with ultrafast control, Nat. Commun. 12 (2021) 5468.
[38] R. Zhao, G.D. Xie, M.L.N. Chen, Z. Lan, Z. Huang, W.E.I. Sha, First-principle calculation of Chern number in gyrotropic photonic crystals, Opt. Express 28 (2020) 4638.
[39] Y.T. Fang, H.Q. He, J.X. Hu, Transforming unidirectional edge waveguide into unidirectional air waveguide, IEEE J. Sel. Top. Quant. 22 (2016), 4901109.
[40] Y.F. Gao, L. He, X.F. Xu, J.P. Sun, Z. Jiang, W.F. Bai, Achievement of unidirectional air waveguide with extra-broad operation bandwidth in magneto-optical photonic crystals with a triangle lattice, J. Magn. Magn. Mater. 496 (2020), 165921.